Fibroblastic Interactions with High-Porosity Ti-6Al-4V Metal Foam

Cheung, Serene; Gauthier, Maxime; Lefebvre, Louis-Philippe; Dunbar, Michael; Filiaggi, Mark

Publisher's version / Version de l'éditeur:
http://dx.doi.org/10.1002/jbm.b.30749
Journal of Biomedical Materials Research Part B: Applied Biomaterials, 82B, 2, pp. 440-449, 2007

NRC Publications Record / Notice d'Archives des publications de CNRC:
http://nparc.cisti-icist.nrc-cnrc.gc.ca/npsi/ctrl?action=rtdoc&an=11343959&lang=en
http://nparc.cisti-icist.nrc-cnrc.gc.ca/npsi/ctrl?action=rtdoc&an=11343959&lang=fr

Fibroblastic Interactions With High-Porosity Ti-6Al-4V Metal Foam

Serene Cheung,[1] Maxime Gauthier,[2] Louis-Philippe Lefebvre,[2] Michael Dunbar,[1,3] Mark Filiaggi[1,4]

[1] School of Biomedical Engineering, Dalhousie University, 5981 University Avenue, Halifax, Nova Scotia, Canada B3H 3J5

[2] Industrial Materials Institute, National Research Council of Canada, 75 de Mortagne Boulevard, Boucherville, Quebec, Canada J4B 6Y4

[3] Department of Orthopaedic Surgery, Queen Elizabeth II Health Sciences Center, 1796 Summer Street, Halifax, Nova Scotia, Canada B3H 3A7

[4] Department of Applied Oral Sciences, Dalhousie University, 5981 University Avenue, Halifax, Nova Scotia, Canada B3H 3J5

Received 16 February 2006; revised 4 October 2006; accepted 4 October 2006
Published online 23 January 2007 in Wiley InterScience (www.interscience.wiley.com). DOI: 10.1002/jbm.b.30749

Abstract: A novel metallic Ti-6Al-4V foam in development at the National Research Council of Canada was investigated for its ability to foster cell attachment and growth using a fibroblast cell culture model. The foam was manufactured via a powder metallurgical process that could produce interconnected porosity greater than 70%. Cell attachment was assessed after 6 and 24 h, while proliferation was examined after 3 and 7 days. Ingrown fibroblasts displayed a number of different morphologies; some fibroblasts were spread thinly in close apposition with the irregular surface, or more often had several anchorage points and extended in three dimensions as they spanned pore space. It was also demonstrated that fibroblasts were actively migrating through the porous scaffold over a 14-day period. In a 60-day extended culture, fibroblasts were bridging and filling macropores and had extensively infiltrated the foams. Overall, it was established that this foam was supportive of cell attachment and proliferation, migration through the porous network, and that it was capable of sustaining a large cell population. © 2007 Wiley Periodicals, Inc. J Biomed Mater Res Part B: Appl Biomater 82B: 440–449, 2007

Keywords: cell culture; fibroblast; titanium (alloys); porosity

INTRODUCTION

Porous cellular frameworks permeate the natural environment and make ideal building blocks for lightweight, mechanically efficient structures. The development of reticulated porous metallic structures could potentially widen the scope of biomedical applications if such scaffolds can successfully anchor implants through tissue infiltration. This method of biological fixation could alleviate some of the stability issues affecting current monolithic designs of hard and soft tissue prosthetics. In addition, the rigidity of a porous structure is a fraction of its solid metallic counterpart, thereby reducing stress-shielding of adjacent tissue, a condition that can contribute to bone resorption with joint replacement devices.

Open-celled metal foams can have pore volumes upwards of 70%, giving a lightweight framework that fills void space by bridging localized defects while providing an environment that facilitates tissue ingrowth.[1] Furthermore, the mechanical behavior of a porous metal remains consistent with time, as opposed to bioresorbable polymers and ceramics that can degrade unpredictably. Anchorage of percutaneous devices, immobilization of porous cardiac pacemaker electrodes, patellar implant stabilization, attachment of tendons or ligaments, filling of large voids, abdominal defect repair, and alveolar ridge augmentation are among the diverse applications for which these materials have been proposed.[2–11]

While commercialization of these porous metal scaffolds has already begun, there have been few *in vitro* studies describing the initial cellular interactions that must occur for eventual tissue infiltration, particularly, with respect to

Correspondence to: M. Filiaggi (e-mail: mark.filiaggi@dal.ca)
Contract grant sponsors: Natural Sciences and Engineering Council of Canada (NSERC)

fibrous tissue. At the cellular level, many cell types have long been observed to respond to topographic surface features ranging in scale from millimeters down to nanometers. The surface morphology is used for orientation and migration, a common example being contact guidance, where the presence of machined grooves causes fibroblasts and other cell types to align themselves and migrate in the direction of the grooves.[12–14] The geometry of focal adhesions presents powerful cues that affect the shape of the cell and the stresses exerted on the cytoskeleton. Cell morphology has been hypothesized to regulate multiple aspects of cell behavior, including growth, gene expression, extracellular matrix production, and differentiation, toward a certain phenotype.[12,15,16] However, the cell response to metal foams in general has not been studied rigorously and, in particular, for the dissimilar foam morphologies that result due to different manufacturing techniques. The objective of the present *in vitro* investigation was to observe the interaction of fibroblasts in short-term and extended culture within a novel three-dimensional porous titanium alloy scaffold.

MATERIALS AND METHODS

Materials Characterization

Ti-6Al-4V Scaffolds. The metal foam scaffolds used in this study were prepared using a proprietary process by the Industrial Materials Institute of the National Research Council of Canada. Ti-6Al-4V metal powder was combined with an organic polymeric binder, a cross-linking agent to cure the binder, and a suitable foaming agent that evolves gas in the temperature range where the binder is liquefied.[17] Foaming was completed at 210°C for 30 min, followed by binder pyrolysis at 425°C for 4 h. The final sintering stage was performed at 1300°C in a repurified argon atmosphere, creating interparticle bonds that consolidated the foam and provided mechanical stability.[17,18]

Ti-6Al-4V foam samples were machined into cylinders measuring 20 mm in length and 15 mm in diameter. The cylinders were sectioned into discs $\sim$1 mm thick using a diamond wafering blade. The discs were then ultrasonicated for 60 min in 70% ethanol to remove particulate debris dislodged during the cutting operation. After sectioning, the discs were sent back to the Industrial Materials Institute for resintering, to consolidate the metal particles and increase mechanical integrity. The resintering treatment consisted of heating the discs in a tube furnace to 1300°C in a repurified argon atmosphere with 1×10^{-7} ppm O_2, holding for 2 h at that temperature. Upon receipt, the porous fraction of each disc was calculated by measuring the mass and thickness. The discs were then numbered and catalogued for tracking purposes during experiments. Prior to cell culture experiments, the foam discs were ultrasonically cleaned in 70% ethanol and sterilized by autoclaving for 20 min at 121°C.

Metallography of Foam Microstructure. Discs were randomly selected for cold mounting in epoxy resin and ground progressively in the order of 120, 240, 400, 600 grit using SiC paper. Samples were then polished using 9-, 3-, and 1-μm diamond suspensions on a polishing cloth. The samples were etched using Kroll's reagent (2 mL HF, 4 mL HNO_3, 94 mL H_2O) by swabbing the surface with gauze until the luster of the metal was dulled. Kroll's reagent preferentially attacks the β-phase, creating topography that enabled the discrimination of the different phases by light microscopy.

Image Analysis of Pore Geometry. To determine cross-sectional porosity, discs were cold mounted in epoxy resin and ground using SiC paper to a 600 grit surface finish. The micrographs were analyzed using the ImageJ freeware program, a Java-based version of NIH Image. Because of the inability of the software to distinguish individual pores, white lines were manually inserted using the Paint program in Windows to differentiate pores from matrix. The adjusted images were then thresholded to identify pore space, and processed accordingly using built-in measurement functions. The jagged, fractal-like pore perimeters were traced quite precisely, but with some measure of subjectivity, by the software algorithms. The pore size was estimated using a descriptor known as Feret's Diameter, which is the largest line segment through a given pore.

Surface Area Determination. The surface area of this porous material was determined by physical gas adsorption using krypton gas. The sample was degassed in a vacuum and cooled to 77 K, and krypton gas was gradually pumped into the chamber and the gas molecules adsorbed to the surface of the foam. The BET equation (after Brunauer, Emmett, and Teller) was used to give the volume of gas needed to form a monolayer on the surface of the sample. The surface area trials were conducted at the National Research Council Steacie Institute for Molecular Sciences in Ottawa using a Quantachrome Quantasorb system for the sorption measurements.

Surface Chemistry Analysis. X-ray photoelectron spectroscopy (XPS) was used to determine the surface composition and elemental oxidation state of autoclaved Ti-6Al-4V foam specimens. The spectra were generated and deconvoluted using a Multilab XPS system with a CLAM4 hemispherical analyzer (VG Microtech). The source was nonmonochromated Mg Kα X-rays bombarded at 15 kV, 20 mA. Quantitative surface composition information was obtained from integrated peak intensities (i.e., area under each peak) and atomic sensitivity factors using the Advantage data acquisition and processing software from Thermo VG Scientific. Peak fits were performed using the Shirley background correction and Gaussian–Lorentzian curve synthesis.

Fibroblast Cell Culture

Immortalized rat fibroblasts (NIH-3T3; American Type Tissue Collection, Manassas, VA) at passages 15–20 were used for experiments. The cells were grown in 75-cm^2 tissue culture flasks in Dulbecco's Modified Eagle's Medium (DMEM) supplemented with 5% fetal calf serum (heat-inactivated at 56°C for 60 min). Cells were passaged twice weekly at 70% confluence, using 2 mL of 0.25% trypsin-EDTA to detach cells, and resuspended in 8 mL of DMEM. Flasks were maintained in a humidified atmosphere at 37°C and 10% CO_2. No antibiotics were used during routine subdivisions or for cell culture experiments to avoid altering cell metabolism.

Fibroblasts for use in experiments were harvested at 70% confluence, detached using trypsin-EDTA, suspended at a concentration of 1×10^5 cells/mL, and verified using a Coulter counter. Five-hundred microliters of cell suspension (corresponding to $\sim$50,000 cells) was inoculated directly onto foam discs contained in a 24-well nontissue culture-treated polystyrene plate. Prior to cell seeding, each disc was prewetted with 500 μL of DMEM for 10 min to prevent air pocket formation within the porous network. The DMEM was removed by vacuum aspiration before the cell suspension was added. The discs were then incubated between 6 h and 60 days for short-term attachment and extended culture studies.

Cellular Interaction With Ti-6Al-4V Foam

Quantification of Cell Attachment and Proliferation. Both cell attachment and proliferation were assessed by counting the number of cells detached by trypsinization using a Coulter counter. The number of adherent cells was measured after 6 and 24 h, while cell growth was determined after 3 and 7 days, with medium changes every third day. For the proliferation studies, the discs were rinsed twice with PBS after 24 h to remove nonadherent and nonviable cells. At the conclusion of each timepoint, the culture medium was carefully removed, and the discs were rinsed twice with 750 μL of PBS to dissociate nonviable and weakly adherent cells. One thousand microliters of 0.25% trypsin-EDTA was added to each disc and gently agitated by pipetting to aid the detachment process and distribute the enzyme throughout the foam. Trypsinization was repeated until counts of less than 1000 cells on the Coulter counter were observed. Cell attachment was expressed as a percentage of trypsinized cells compared with the original 50,000 cells seeded, while cell growth was expressed as the percent difference in cell number at 72 h or 1 week compared with the average number of cells attached at 24 h [e.g., % growth = (number of cells at 1 week − number of attached cells at 24 h) × 100%/number of attached cells at 24 h].

Assessment of Cell Viability. The MTT colorimetric assay was used to evaluate the viability of the cell population after 7 days. A 5 mg/mL solution of MTT reagent was prepared in phosphate-buffered saline and sterile-filtered. MTT reagent (50 μL) was added to each disc and incubated for 4 h in 10% CO_2 at 37°C. The discs were then examined under a light microscope to verify that the incubation time was sufficient for crystal formation. The formazan crystals were dissolved in 100 μL of solubilization solution, composed of 1% Triton-X 100 detergent and 0.01*N* HCl in isopropanol. After gentle stirring on a rotating table for 2 h, 50 μL was sampled from each well and placed in a 96-well plate. The absorbance was read at 570 nm on a multidetection microplate reader.

Cell Migration. Individual discs were placed into a stack to approximate a monolithic piece of foam, ensuring the faces were in contact to permit cell movement from one disc to another. At the conclusion of the experiment, the discs were simply separated from one another and cells detached from each disc with trypsin. The top disc of each three-disc stack was seeded with 100,000 cells and incubated for 24 h. After a rinse to remove unattached cells, this disc was placed on top of two cell-free discs, each $\sim$1 mm thick, and incubated in a 24-well plate for 14 days (3 stacks of 3 discs each). One milliliter of cell culture medium was added to each stack and changed every 3 days. The cells were kept in a 37°C humid environment maintained at 10% CO_2. At the end of the test, the discs were transferred separately to clean wells with sterile tweezers. The cell counting process consisted of adding 1 mL of 0.25% trypsin-EDTA to each disc, followed by a rinse with 1 mL of PBS. Cell counts were quantified in duplicate using the Coulter counter.

Cell Distribution by Confocal Microscopy. After a 24 h incubation, the cell-seeded discs were fixed in 3% paraformaldehyde for 30 min, rinsed twice with PBS, and the fibroblasts were fluorescently labeled using rhodamine–phalloidin to stain the cytoskeletal actin filaments. The discs were rinsed twice and stored in PBS in a 24-well plate wrapped in aluminum foil and refrigerated to prevent degradation of the fluorescent probe. For viewing, the samples were removed from the PBS and placed carefully on top of a no. 0 thickness glass coverslip. Images were captured using the 10× objective lens on a Zeiss LSM 510 laser scanning confocal microscope with the HeNe laser set to a wavelength of 633 nm to correspond with red fluorescence. The digitized images were manipulated using the 3D for LSM software package included with the instrument system.

Cell Morphology by Scanning Electron Microscopy. At 3 or 6 days of culture, fibroblast-containing discs were prepared for visualization on the scanning electron microscope (SEM). The cells were fixed in 2.5% glutaraldehyde for 2 h, rinsed 3 times in sterile PBS, and immersed in 4% OsO_4 for 1 h for additional stabilization and improved contrast. The discs were rinsed 3 times in sterile PBS, followed by graded

DOI 10.1002/jbmb

ethanol dehydration in the order of 25, 50, 70, 80, 90, 100%. Final dehydration was completed in hexamethyldiasilazane, a wet chemical method that preserves cellular structures similarly to critical point drying but allows for preparation of larger specimens.[19,20] Samples were viewed in a Hitachi S-4700 cold field emission SEM. The foam specimens were attached onto an aluminum stub using double-sided copper tape. Accelerating voltages ranged between 1 and 15 kV with emission currents at 10–30 μA, and a sample working distance of 12–13 mm. Images were captured in digital format at magnifications from 50 to 5000× in secondary electron detection mode.

RESULTS

Foam Disc Characterization

From manual measurements of disc dimensions and mass ($n = 290$), the foams averaged 0.2239 ± 0.0324 g in mass, 1.085 ± 0.141 mm in thickness, and 71.76% ± 2.42% in porosity. Disc diameter was constant at 14.5 mm due to precision machining of the foam cylinders during sample manufacture. From krypton gas adsorption porosimetry, the normalized surface area was 0.0356 m^2 per gram of foam. Applying this to the measured mass of the discs, the surface area averaged 79.7 ± 11.5 cm^2 for the disc population. In comparison, there is only 3.75 cm^2 of available surface area on an equivalent polished solid disc (14.5 mm diameter, 1 mm thick), so the porous scaffold contained 20 times more available surface area for cell attachment and ingrowth.

Image analysis of three representative polished foam cross-sections was used to estimate the pore size distribution. Sixty-three micrographs were digitally captured and a total of 1905 pores were distinguished from the thresholded images [Figure 1(a)]. These pores ranged in size from 3 to 1650 μm according to Feret's diameter. As shown in the histogram [Figure 1(b)], 50% of the pores was smaller than 50 μm and 85% of the pores was less than 200 μm.

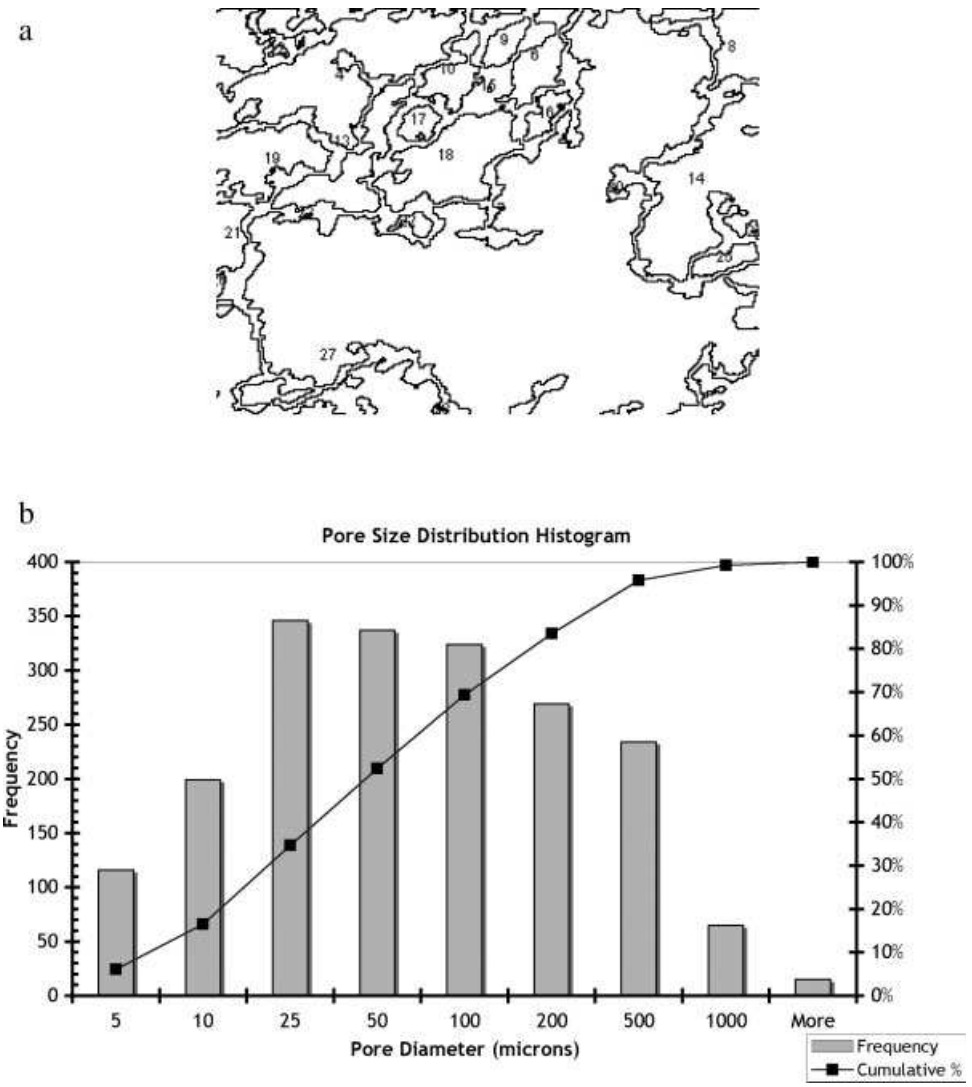

Figure 1. Pore size estimation by image analysis. (a) Edited image with pore separation and resultant porosity analysis; (b) cumulative pore size distribution histogram.

Detailed visual examination of the foam was conducted by SEM before inoculation with cells. The morphological analysis revealed its complex architecture and three-phase porosity developed during manufacturing. The pores were interconnected and randomly distributed in this three-dimensional network. All three levels of porosity were encompassed in this image of the Ti-6Al-4V foam, which included large macropores, intermediate pore space, and fine micropores between the sintered particles [Figure 2(a–c)]. Higher magnification viewing of the resintered structure revealed numerous regions containing thermal etching lines that are characteristic of titanium vacuum-sintered at high temperature.[21]

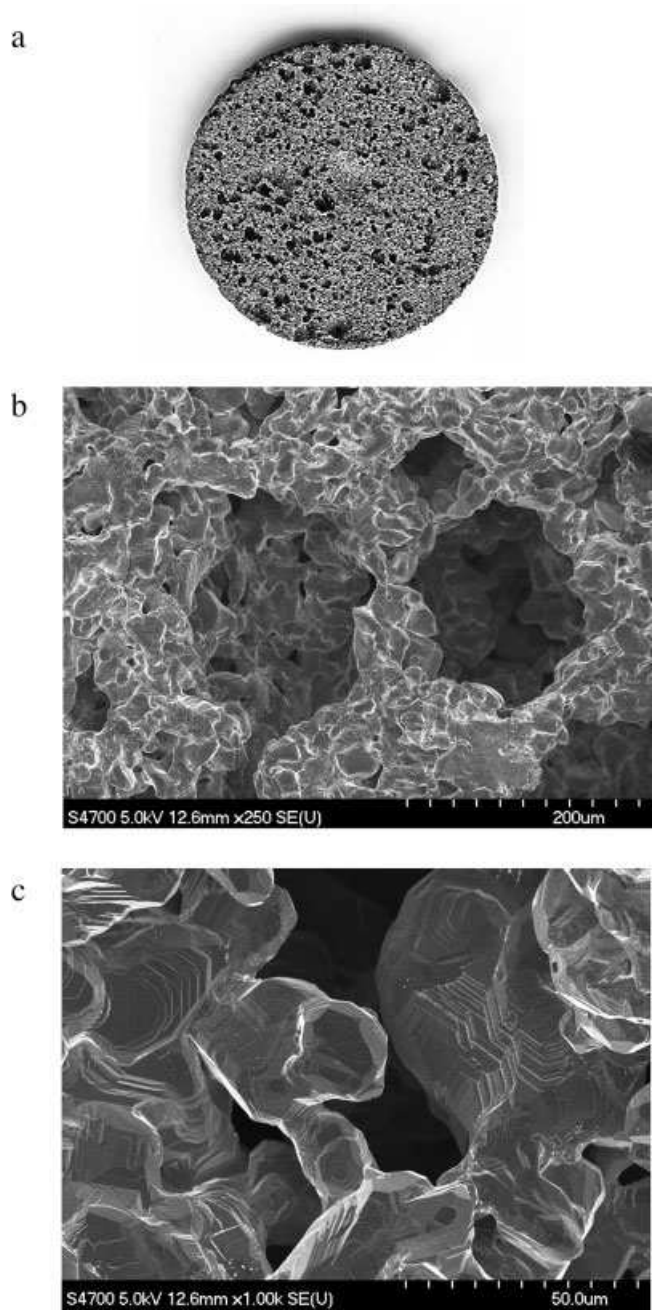

Figure 2. Foam morphology and surface characteristics. (a) Macroscopic image of foam disc; (b) low-magnification SEM micrograph of metal foam; (c) thermal etching lines on foam facets.

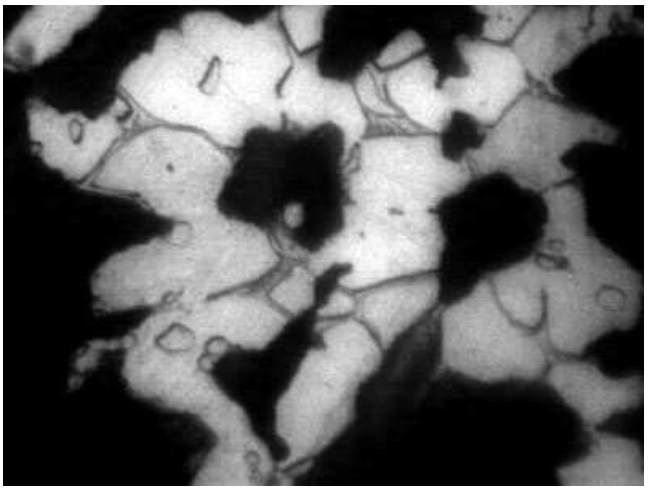

Figure 3. Etched microstructure of Ti-6Al-4V foam showing primary α phase, with β phase in the grain boundaries.

Examination of the foam microstructure revealed mostly the light primary α-phase in the form of large, globular grains with very limited amounts of dark retained-β phase seen in grey between the α grains (Figure 3). The epoxy resin used to mount the samples appears in black. For the evolution of this microstructure, the cooling rate must have been extremely slow to have allowed the nucleation and growth of the primary α grains without the formation of basket-weave or Widmanstätten structures from the β phase composition obtained at 1300°C.[22] Because there was such a small fraction of retained β phase, vanadium could be heavily concentrated within these regions, since it normally segregates to the β phase.

Chemical analysis of the surface by XPS detected titanium, carbon, oxygen, aluminum, and vanadium-containing compounds on the foam surfaces (Table I). The atomic percentages for each element were generally in good agreement with the findings of other studies for Ti-6Al-4V,[23–27] suggesting that the foam behaved similarly to solid bar stock after autoclaving. Titanium was the metal detected at the highest concentration, followed by aluminum and vanadium. TiO_2 was detected along with Ti_2O_3 in approximately equal amounts, indicating a mixed oxide composition. High levels of carbon were detected due to adsorbed organic contaminants, primarily hydrocarbons in the form of $—CH_x—$, C—O, and C=O bonded species. However, levels of 20–30% are typical even for well-cleaned surfaces that have spent time in ambient air.[27] Oxygen-containing compounds were the dominant chemical species, but because of the high vacuum conditions under which the XPS measurements were performed, the percentages of water-based groups (OH and OH_2) may have been artificially decreased with their removal under high vacuum.[28] Significant aluminum enrichment ($\sim$23 wt % or $\sim$35 at %

DOI 10.1002/jbmb

TABLE I. Surface Chemistry Analysis of the Ti-6Al-4V Foam Disc by XPS

	Binding Energy (eV)	Composition (at %)
$Ti_{2o3/2}$		12.39
Ti (O_2)	458.2	6.69
Ti ($_2O_3$)	457.7	5.70
C_{1s}		23.30
Hydrocarbons (C—C)	284.5	12.30
C—O	286.2	5.13
C=C	288.2	4.57
C—O—O	290.7	0.80
O_{1s}		55.71
O^{2-}	529.5	37.67
OH or C=O	531.1	11.38
OH_2 or C—O	532.4	5.05
Other	534.1	1.62
Al_{2p}		7.29
Al ($_2O_3$)	74.0	4.59
Native Oxide	75.9	1.63
Other	77.4	1.08
$V_{2p3/2}$		1.31
V ($_2O_5$) or (O_2)	516.3	0.90
V ($_2O_3$)	524.7	0.41

when considering the total metallic content only) was seen in the oxide relative to the bulk alloy. Such enrichment has been noted by other researchers,[23,26,27,29–31] and may have been accentuated by the heat involved in autoclaving.[27] The aluminum was predominantly present in the most stable 3+ state corresponding to Al_2O_3, as indicated by a 74.0 eV binding energy for Al. Vanadium present as mixed oxides (VO_2, V_2O_5, and V_2O_3) was also noted at levels exceeding the bulk alloy composition, contrary to several reports of V deficiency in the surface oxide of these alloys.[23,26,27,29–31] Autoclaving may have accounted as well for some of this unexpected enrichment. However, it is also plausible that an overlap of the main V2p photoemission signal and an O1s satellite, as is observed with XPS when using nonmonochromatized radiation,[27] may have confounded subsequent quantitative peak analysis.

Cell Attachment and Distribution

After 6 h, slightly less than 50% of inoculated cells had attached to the surface of the foam (46% ± 3%, $n = 6$). A sizeable portion of the fibroblasts remained clustered around the edge of the disc, having fallen through the pores when the cell suspension was applied to the foam. After 24 h, however, the number had dropped to 38% ± 3% ($n = 6$), a small but significant decrease despite the longer incubation period ($p = 0.002$, Student t test, equal variances). Notably, no correlation was seen between cell attachment efficiency and disk characteristics (surface area, thickness, or % porosity) for either time point (data not shown).

Because the foam was not translucent, there were limitations on cell visualization by conventional light microscopy. Laser scanning confocal microscopy enabled the imaging of fluorescent fibroblasts within the scaffold, allowing for an estimate of the depth of distribution and cell spacing after initial seeding. A representative image of red, actin-stained fibroblasts attached to an "invisible" foam matrix is shown in Figure 4. The cells were quite sparsely distributed, and few cell-to-cell contacts were observed. The fibroblasts also appeared to be in different stages of spreading, with some already assuming a stellate or spindle morphology and revealing points of anchorage. Other cells were rounded, which may have been because they were in the process of mitosis, had not fully spread, or because they were adhered flush to the faces of the foam microstructure. By adjusting the microscope focus and locating cells at increments of 20 μm, it was determined that cells had been dispersed up to 570 μm deep into the foam after 24 h.

Cell Proliferation and Viability

By day 3 the cells had sufficiently recovered after removal of nonviable cells at 24 h to post an average percent growth of 113% ± 34% ($n = 9$), effectively doubling the cell population remaining attached after 24 h. This proliferative response continued out to day 7, yielding an average percent growth of 776% ± 132% ($n = 8$) relative to the number of initial attached cells. An MTT assay performed at day 7 confirmed this favorable response. Based on average absorbance value of 0.336 ± 0.027 ($n = 6$), and applying the equation of the calibration curve to correlate absorbance with cell number ($y = 599612x$, $R^2 = 0.9806$),

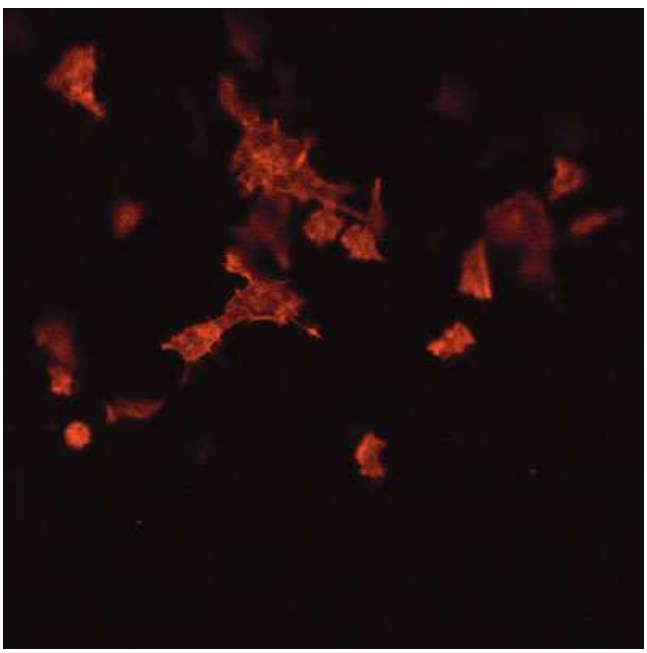

Figure 4. Confocal microscope image illustrating cell morphology (10× objective lens with 2× optical zoom) after a 24-h culture. [Color figure can be viewed in the online issue, which is available at www.interscience.wiley.com.]

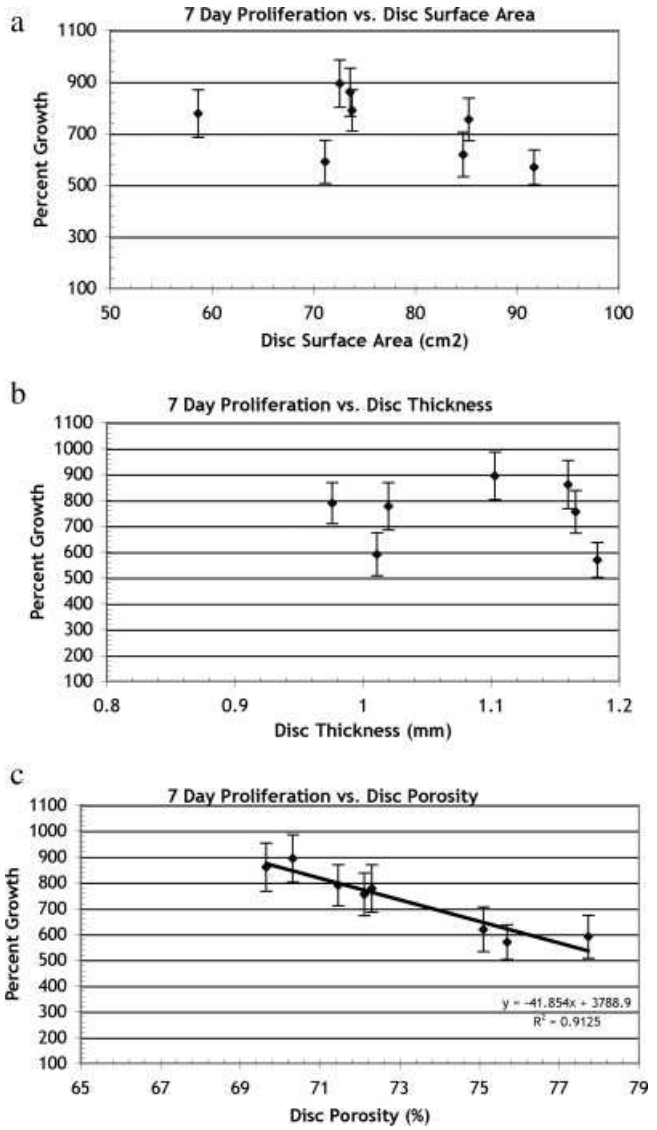

Figure 5. Scatter plots relating day 7 cell proliferation and (a) disc surface area, (b) disc thickness, and (c) percent porosity.

this translated to growth of 960% ± 86% (relative to the number of attached cells after 24 h), falling within the range of the cell count data.

An assessment of disc characteristics and cell growth was conducted with 7-day discs. The data were scattered quite randomly in the plots of percent growth versus disc surface area and thickness [Figure 5(a,b)]. Regression in Microsoft Excel did not produce correlation coefficients above 0.7 using linear, polynomial, or logarithmic curve-fitting models for any of the data sets. For the porosity comparison, however [Figure 5(c)], there appeared to be an inverse linear relationship between percent growth and porosity ($R^2 = 0.9125$). There was no definitive explanation for this observation, aside from possible differences in macropore and micropore distribution in the foams that may have influenced nutrient and oxygen transport and subsequent cellular growth and infiltration.

Fibroblast Morphology

Cells were fixed after 3 and 6 days of culture for imaging, to evaluate their morphology and attachment behavior on the foam substrate. The fibroblasts were anchored somewhat precariously onto the facets of the foam, appearing to accommodate the irregularly shaped three-dimensional surface topography, while in some cases spanning pore space. Focal adhesions were prominent if the cell was spanning pore space, otherwise, fibroblasts assumed a thinly spread shape to adhere in close apposition to the facets in the foam microstructure [Figure 6(a)]. Cell morphology was quite variable depending on the points of anchorage, including shapes that can be described as rounded/polygonal, spindle/bipolar, triangular, and stellate/star-like or multipolar.

Although the cells were seeded sparsely throughout the foam, as shown in the fluorescent confocal microscope images, the rate of proliferation presumably accelerated on these discs once more cell-to-cell contacts were established. On day 3, fibroblasts were still scattered and difficult to locate on the surface of the foam discs. By day 6, cells were far more prevalent and tended to form regions of increased

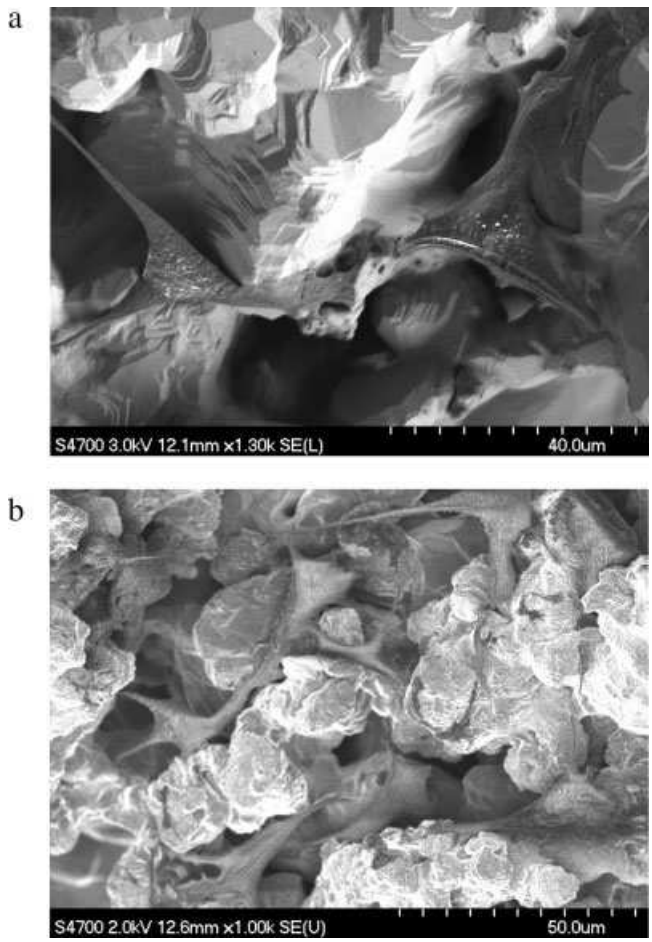

Figure 6. Fibroblast morphology as anchored within the foam microstructure. (a) At day 3, showing focal adhesions and cell spreading; (b) at day 6, illustrating a region of increased cell density.

DOI 10.1002/jbmb

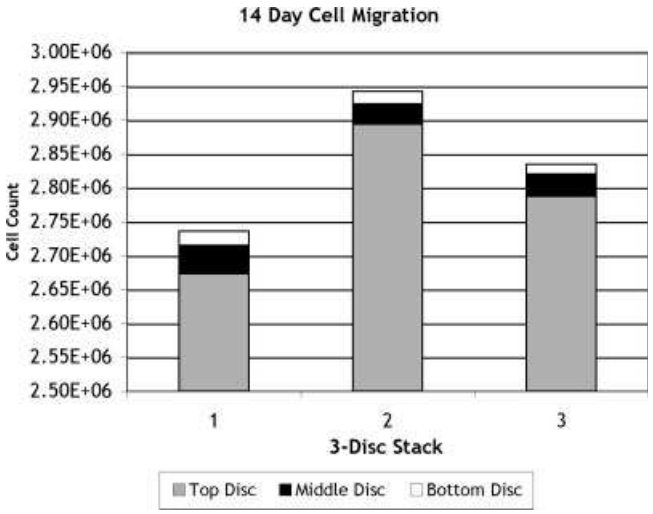

Figure 7. A semiquantitative determination of cell migration by measuring cell distribution within a three-disc stack model. The top disc was seeded with 100,000 cells and cultured overtop two additional discs for 14 days. The results for 3 three-disk stacks are shown. For any one disk, cell counts were highly reproducible (SDs of 1.6–4.4%).

cell density, although the individual fibroblasts remained well spread as opposed to grouping in clusters [Figure 6(b)].

Cell Migration

The starting cell concentration was raised to 100,000 cells seeded on the top disc to facilitate cell proliferation by permitting more cell-to-cell contact within the foam. Remarkably, growth on the top discs averaged over 2700% after 14 days. This growth pattern may have signified a preference for the fibroblasts to colonize the seeded top disc and form a cell monolayer instead of migrating through the scaffold. Cell movement was indeed observed, but only a fraction of the total cell population was detected beyond the top disc (Figure 7).

Extended Culture

Two foam discs were maintained *in vitro* for long-term observations of cell growth and infiltration of the matrix. Light microscope images documented the gradual colonization of the foam over the 60-day period. At 14 days, there was evidence of cell monolayer bridging of open pore space, with rapid increases in cell number observed qualitatively after 30 days. By this point, there was significant filling of macropores from the outside inward by cell multilayers. Pore filling continued to increase with time, but by day 40, there was noticeable cell migration from the disc onto the bottom of the tissue culture plastic flask, as the foam was becoming saturated with cells. Routine medium changes were so frequent at this point that the discs were transferred from the 24-well plate to a 75-cm^2 flask with 20 mL of DMEM to decrease the risk of contamination and infection during handling. After 60 days, some macropores were completely filled through the entire 1 mm thickness, with substantial cell migration onto the plastic only 3 days after the discs were transferred to a new flask.

DISCUSSION

This study has illustrated the response of fibroblasts cultured *in vitro* within a three-dimensional porous scaffold having complex surface topography. The adaptive capabilities of the cells were aptly demonstrated on this substrate, with its uneven topography, rough facets, and variable pore size. Fibroblasts were able to anchor and adapt accordingly to the shape of metal particles, spanning three-dimensionally open porosity in some cases. Slightly less than half of inoculated cells successfully attached to the foam surface using a starting population of 50,000 fibroblasts. However, the resultant cell attachment rate could have been dependent upon the initial seeding density, an aspect not investigated within the scope of this study. After 7 days of incubation, remarkable proliferation was observed. The foam was also able to sustain a large cell population over a 60-day period, as the fibroblasts colonized the material and began to fill the pores. While these results were achieved without surface treatment, coating the metal foam with collagen or proteins such as fibronectin could produce very interesting cell–material interactions worthy of subsequent research.

Although comparative experiments could have been performed on polished or roughened solid Ti-6Al-4V discs, a number of factors related to the properties of the foam discs complicated the design of such trials. Differing processing and heat treatment histories between the foam and Ti-6Al-4V bar stock would have led to the development of dissimilar α- and β-phase microstructures, as well as corresponding differences in surface chemistry. The foam discs also varied in mass and therefore in the amount of available surface area for cell attachment; a difference of only 0.01 g in mass of any given disc would be reflected as 3.5 cm^2 of surface area. A broad pore size distribution [Figure 1(b)] and the interconnectedness of the pore network further influenced the efficiency with which cells could be seeded onto these foams, with a significant fraction of cells in the suspension flowing through the pores and being "lost" during the inoculation procedure. From the 4-h attachment data, $\sim$50% of the seeded fibroblasts did not attach to the substrate, and much of this can be attributed to the open porosity of the discs. Attempts were made to perform a numeric reconciliation (cells in = cells out), but unattached cells were observed to form large clumps at the perimeter of the nontissue culture-treated polystyrene wells and could not be effectively separated into single cells despite liberal use of trypsin and agitation. Presumably, "flow-through" would not be an issue with *in vivo* studies where endogenous cells would be expected to populate the scaffold.

Overall, no clear relationship between disc characteristics and cell attachment or growth was elucidated. While a

moderate inverse linear relationship between percent growth and porosity was observed, it should be noted that porosity was determined gravimetrically and was not indicative of the pore size distribution. Discs alike in gravimetric porosity did not necessarily share a similar macropore/micropore size profile, which could be a more influential determinant to cellular ingrowth and proliferation. Importantly, these responses were also obtained using an immortalized cell line that may not wholly reflect the behavior of human-derived cells *in vitro* or, ultimately, *in vivo*. Nonetheless, the pore size distribution of this foam could be favorable for fibrovascular ingrowth, which is purportedly the type of tissue that develops *in vivo* when pore sizes are between 15 and 50 μm.[32] Fibrous tissue has also been shown to readily heal when pores are greater than 50 μm,[33] and 45% of the pores was larger than this value. However, 20% of pore distribution was below 10 μm and this significant fraction could be inaccessible to cells, being smaller in scale than an average spread-out fibroblast.

Cell migration is an area of interest for porous biomaterials, where the interconnected pore space is designed to encourage the movement of cells through the foam. The difficulty with quantifying the extent of cell migration lies within the design of a suitable experiment. Although it represents the ideal situation, the use of one thick cylinder of foam presents an obstacle when attempting to count cells or perform relevant assays. There is no conceivable method of sectioning the foam without removing attached cells in the process, nor is it possible to determine how far the cells have migrated through the cylinder without destroying the sample and the cells within. Light and electron microscopy are limited in their penetration depth and would not be able to view the interior of the foam.

This experimental design circumvented these issues and more importantly allowed a reliable estimate of the extent and distance covered by migrating cells through the porous network. With a stacked-disc model consisting of three discs, it was possible to gauge the movement of cells through the foam microstructure and assess the interconnectivity of the pore network. Because the thickness of each disc was known, the distance traveled by the cells through the foam could be approximated in discrete terms. The innately high porosity of the foam likely minimized any obstruction of pores. Nevertheless, any potential misalignment of the pores or gaps at the disc interfaces could have presented barriers to cell migration. Overall, limited cell movement was observed out of the top cell-seeded disc into the two discs below. If the culture period was extended beyond 2 weeks, migrating cells may have been apparent in larger numbers. The shift to a larger pore size distribution could have also increased the rate of cell migration above what was recorded. As well, the cells were moving against the oxygen gradient by going deeper within the foam, where oxygen concentrations were lower than on the surface of the top disc. If the culture medium was circulated in a perfusion system, it is highly probable that fibroblasts would be more apt to migrate. That a significantly smaller cell population was observed in the two bottom disks after 2 weeks of culture may also be a reflection of the inability of fibroblasts to undergo mitosis during *active* migration, leading to some delay or attenuation in cell growth relative to less peripatetic cells. Nevertheless, the confirmed movement of cells over a distance of 2 mm through the foam scaffold established that this porous network was interconnected and conducive to cell migration.

CONCLUSIONS

The Ti-6Al-4V foam produced by the Industrial Materials Institute of the National Research Council was a biocompatible scaffold, supportive of cell attachment, proliferation, and infiltration in extended *in vitro* culture. Successful multilayered cellular ingrowth of the porous scaffold was observed over 60 days, suggesting that the foam was capable of sustaining a large viable cell population. Further research into cellular interactions and possible implantation into a small animal model should be undertaken to evaluate the suitability of this material for future orthopaedic or soft tissue applications.

The authors thank Dr. Jonathan Blay in the Department of Pharmacology (Dalhousie University) for his cell culture expertise and Dr. Michael Gharghouri in the Department of Mining and Metallurgical Engineering (Dalhousie University) for assistance with the SEM. Gratitude is also extended to Ms. Maxine Langman and Mr. Gordon Hall from the Department of Applied Oral Sciences for their technical assistance. The Canada Foundation for Innovation and the Atlantic Innovation Fund provided support for the "Facilities for Materials Characterization" managed by the Institute for Research in Materials, Dalhousie University.

REFERENCES

1. Zardiackas LD, Parsell DE, Dillon LD, Mitchell DW, Nunnery LA, Poggie R. Structure, metallurgy, and mechanical properties of a porous tantalum foam. J Biomed Mater Res 2001;58:180–187.
2. Hacking SA, Bobyn JD, Toh K, Tanzer M, Krygier JJ. Fibrous tissue ingrowth and attachment to porous tantalum. J Biomed Mater Res 2000;52:631–638.
3. Schultz P, Vautier D, Egles C, Debry C. Experimental study of a porous rat tracheal prosthesis made of T40: Long-term survival analysis. Eur Arch Otorhinolaryngol 2004;261:484–488.
4. Schultz P, Vautier D, Chluba J, Marcellin L, Debry C. Survival analysis of rats implanted with porous titanium tracheal prosthesis. Ann Thorac Surg 2002;73:1747–1751.
5. Jansen JA, Walboomers XF. A new titanium fiber mesh-cuffed peritoneal dialysis catheter: An experimental animal study. J Mater Sci Mater Med 2001;12:1033–1037.
6. Walboomers F, Paquay YC, Jansen JA. A new titanium fiber mesh-cuffed peritoneal dialysis catheter: Evaluation and comparison with a Dacron-cuffed tenckhoff catheter in goats. Perit Dial Int 2001;21:254–262.
7. Paquay YC, de Ruijter JE, van der Waerden JP, Jansen JA. Wound healing phenomena in titanium fibre mesh: The influence of the length of implantation. Biomaterials 1997;18:161–166.

8. Paquay YC, de Ruijter JE, van der Waerden JP, Jansen JA. Tissue reaction to Dacron velour and titanium fibre mesh used for anchorage of percutaneous devices. Biomaterials 1996;17: 1251–1256.
9. Eisig SB, Ho V, Kraut R, Lalor P. Alveolar ridge augmentation using titanium micromesh: An experimental study in dogs. J Oral Maxillofac Surg 2001;61:347–353.
10. Bobyn JD, Wilson GJ, MacGregor DC, Pilliar RM, Weatherly GC. Effect of pore size on the peel strength of attachment of fibrous tissue to porous-surfaced implants. J Biomed Mater Res 1982;16:571–584.
11. MacGregor DC, Wilson GJ, Lixfeld W, Pilliar RM, Bobyn JD, Silver MD, Smardon S, Miller SL. The porous-surfaced electrode: A new concept in pacemaker lead design. J Thorac Cardiovasc Surg 1979;78:281–291.
12. Schakenraad JM. Cells: Their surfaces and interactions with materials. In: Ratner BD, Hoffman AS, Shoen FJ, Lemons JE, editors. Biomaterials Science: An Introduction to Materials in Medicine. San Diego, CA: Academic Press; 1996. pp 141–147.
13. Boyan BD, Hummert TW, Dean DD, Schwartz Z. Role of material surfaces in regulating bone and cartilage cell response. Biomaterials 1996;17:137–146.
14. Lausmaa J. Mechanical, thermal, chemical and electrochemical surface treatment of titanium. In: Brunette DM, Tengvall P, Textor M, Thomsen P, editors. Titanium in Medicine. Germany: Springer Verlag; 2001. pp 232–258.
15. Wieland M, Chehroudi B, Textor M, Brunette DM. Use of Ti-coated replicas to investigate the effects on fibroblast shape of surfaces with varying roughness and constant chemical composition. J Biomed Mater Res 2002;60:434–444.
16. Chou L, Firth JD, Uitto VJ, Brunette DM. Substratum surface topography alters cell shape and regulates fibronectin mRNA level, mRNA stability, secretion and assembly in human fibroblasts. J Cell Sci 1995;108 (Part 4):1563–1573.
17. Lefebvre L, Thomas Y. Method of making open cell material. US Pat. No. 6, 660, 224, 2003.
18. Lefebvre L, Gauthier M, St. Pierre JP, Bureau MN. Development of titanium foams for tissue attachment. In: Transactions of 29th Annual Meeting Society for Biomaterials, Reno, NV, 2003. p 325.
19. Braet F, De Zanger R, Wisse E. Drying cells for SEM, AFM and TEM by hexamethyldisilazane: A study on hepatic endothelial cells. J Microsc 1997;186 (Part 1):84–87.
20. Bray DF, Bagu J, Koegler P. Comparison of hexamethyldisilazane (HMDS), Peldri II, and critical-point drying methods for scanning electron microscopy of biological specimens. Microsc Res Tech 1993;26:489–495.
21. Pilliar RM. Porous-surfaced metallic implants for orthopedic applications. J Biomed Mater Res 1987;21 (A1, Suppl):1–33.
22. Pederson R. Microstructure and Phase Transformation of Ti-6Al-4V. Sweden: Lulea University of Technology; 2002.
23. MacDonald DE, Rapuano BE, Deo N, Stranick M, Somasundaran P, Boskey AL. Thermal and chemical modification of titanium-aluminum-vanadium implant materials: Effects on surface properties, glycoprotein adsorption, and MG63 cell attachment. Biomaterials 2004;25:3135–3146.
24. Lin H, Bumgardner JD. Changes in surface composition of the Ti-6Al-4V implant alloy by cultured macrophage cells. Appl Surf Sci 2004;225:21–28.
25. Deligianni DD, Katsala N, Ladas S, Sotiropoulou D, Amedee J, Missirlis YF. Effect of surface roughness of the titanium alloy Ti-6Al-4V on human bone marrow cell response and on protein adsorption. Biomaterials 2001;22:1241–1251.
26. Zreiqat H, Howlett CR. Titanium substrata composition influences osteoblastic phenotype: In vitro study. J Biomed Mater Res 1999;47:360–366.
27. Textor M, Sittig C, Frauchiger V, Tosatti S, Brunette DM. Properties and biological significance of natural oxide films on titanium and its alloys. In: Brunette DM, Tengvall P, Textor M, Thomsen P, editors. Titanium in Medicine. Germany: Springer Verlag; 2001. pp 172–224.
28. Kilpadi DV, Lemons JE, Liu J, Raikar GN, Weimer JJ, Vohra Y. Cleaning and heat-treatment effects on unalloyed titanium implant surfaces. Int J Oral Maxillofac Implants 2000;15: 219–230.
29. Ask M, Lausmaa J, Kasemo B. Preparation and surface spectroscopic characterization of oxide films on Ti-6Al-4V. Appl Surf Sci 1989;35:283–301.
30. Sodhi RNS, Weninger A, Davies JE, Sreenivas K. X–ray photoelectron spectroscopic comparison of sputtered Ti, Ti-6Al-4V, and passivated bulk metals for use in cell-culture techniques. J Vac Sci Technol A 1991;9:1329–1333.
31. Okazaki Y, Tateishi T, Ito Y. Corrosion resistance of implant alloys in pseudo physiological solution and role of alloying elements in passive films. Mater Trans 1997;38:78–84.
32. Kaplan RB. Open cell tantalum structures for cancellous bone implants and cell and tissue receptors. US Pat. No. 5, 282, 861, 1994.
33. Hacking SA, Tanzer M, Harvey EJ, Krygier JJ, Bobyn JD. Relative contributions of chemistry and topography to the osseointegration of hydroxyapatite coatings. Clin Orthop Relat Res 2002;405:24–38.